Biofidelity Assessment of a GHBMC M50 in Rear-Facing Seating Configuration during a High-Speed Frontal Impact

V. Pradhan[1], R. Ramachandra[2], J. Stammen[3], K. Moorhouse[3], J. Bolte IV[1], Y.S. Kang[1]
[1] The Ohio State University; [2] Transportation Research Center, Inc., [3] National Highway Traffic Safety Administration/VRTC

ABSTRACT

Automated driving systems (ADS) may be used in future vehicles, which would relieve the occupants of the driving task. Thus, non-conventional seating configurations have been proposed. One of the configurations that the customer may want for a long duration journey is rear-facing for front-row occupants, but the safety of this configuration needs to be explored further. Finite element (FE) human body models (HBM) could potentially be used to assess rear-facing occupant safety in vehicles equipped with ADS. However, they have not been validated in this scenario. The objective of this study is to evaluate the biofidelity of the Global Human Body Models Consortium 50th percentile male detailed model (GHBMC M50-O) in a rear-facing seat with 25 seatback recline angle, in a high-speed (56km/h) frontal impact scenario using biomechanical corridors from post-mortem human subjects (PMHS) experiments (Kang et al., 2020). Prior to biofidelity evaluation of the GHBMC, an effort was made to validate the seat using unoccupied seat responses and Hybrid III 50th percentile male (H3) responses. The total seatback loads from both unoccupied seat and H3 simulations had a normalized root mean squared deviation (NRMSD) less than 10% from experimental seatback loads, indicating a fairly-validated seat with the possibility of further improvements. The biofidelity of the GHBMC was evaluated using the NHTSA Biofidelity Ranking System (BRS). The GHBMC exhibited good (BRS≤1) to moderate (1<BRS≤2) biofidelity for the rotational kinematics of the head and thoracic spine, but poor biofidelity for their displacements in the x-axis direction (BRS>2), likely due to GHBMC limitations in spine and surrounding soft-tissue modeling or unrealistic seat foam behavior. The pelvis and lower extremities of the GHBMC exhibited poor biofidelity in rotational kinematics (BRS>2), which might indicate the necessity for improving the pelvis and lower extremity portions of the model.

INTRODUCTION

Future vehicles equipped with automated driving systems (ADS) are likely to utilize non-traditional seating configurations. A survey study by Jorlöv et al. (2017) identified rear-facing seats as a popular configuration for front-row occupants, where they can engage in conversations with second-row forward-facing occupants during long drives. However, conventional restraint systems like the airbag and seatbelt that were optimized for upright forward-facing occupants might be insufficient in protecting rear-facing occupants during a motor vehicle crash (MVC). Therefore, it is necessary to further explore vehicle occupant safety in the rear-facing seating

scenarios. FE HBMs are becoming more frequently utilized as a part of virtual testing to assess biomechanical responses and injury risk to occupants. Once they are evaluated under all impact severities and deemed biofidelic, they may be used to evaluate responses in various restraint conditions to limit the need for extensive physical testing. Kitagawa et al. (2017) used the Total Human Model for Safety (THUMS) finite element model in a high-speed rear-facing seating scenario, in which the Neck Injury Criteria (Nij) and upper chest deflection values were higher than those from other seating scenarios, reflecting the injury potential in the rear-facing seating scenario. However, the THUMS model has only been validated in low-speed rear impact. The Global Human Body Models Consortium (GHBMC) M50 model has been previously evaluated in moderate-speed (24km/h) rear impacts, with the models exhibiting post-mortem human subjects (PMHS)-like gross kinematics, with good biofidelity in the head to T1 region (Katagiri et al., 2019), although the head and neck of the GHBMC was validated in low-speed (<17 km/h) rear impacts (Fice et al, 2011). Kang et al. (2020) observed multiple rib fractures and some pelvis injuries in the PMHS tested in the high-speed rear-facing seating scenarios. The GHBMC models may be able to provide valuable information that could not be seen in PMHS tests, such as occupant-seat interaction, rib deformation patterns, and pelvis deformation after the models are evaluated and validated in the high-speed rear-facing scenarios.

Therefore, the main objective of this study is to evaluate biofidelity of GHBMC in the high-speed (56km/h) rear-facing configuration during frontal impact simulations at 25 degree seatback recline angles using the biomechanical corridors from the Kang study.

METHODS

An FE model of an original equipment manufacturer (OEM) seat with an All-Belts-To-Seat (ABTS) seatbelt system (TS Tech Americas, Inc) and the GHBMC M50 model were used to simulate occupant responses in a high-speed rear-facing frontal impact. Simulations were performed using the general purpose multi-physics simulation software package LS-DYNA v11.0.0 (Livermore Software Technology Corporation).

Sled Setup

The geometry of the seatback structure used in the unoccupied seat experiments (Kang et al., 2020) was obtained from FARO laser scan of the experimental sled. However, only the geometry of the plates contacting the seatback and the attached load cells were considered to simplify the FE model (Figure 1a). Solid meshing was performed on the geometry with a biased mesh on the interface of the plates and the load cells to have nodal connectivity. Material properties of steel were applied to the structure. Cross sections consisting of a node set and an element set were defined in the center of each load cell, and reaction loads were quantified as sum of nodal forces from these cross sections (Figure 1a) (White et al., 2015). The physical seat was scanned and FARO was taken from the seat mounted on the sled to obtain the position and the angle of the seatback structure. The seatback structure and the seat anchors were attached to the floor using constrained extra nodes (Figure 1b).

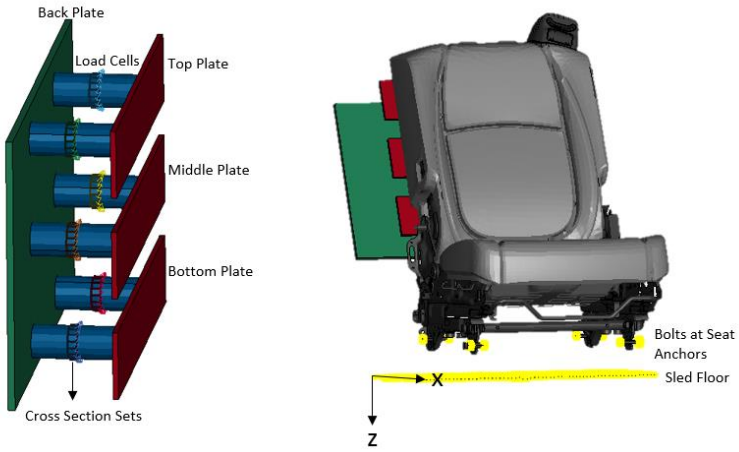

(a) Seatback structure. (b) Seat-floor connection.

Figure 1: Sled setup used in the simulations.

A high-severity pulse (peak acceleration=37g, delta V=56km/h) used in the experiment, as shown in Figure 2, was prescribed to the sled floor in the simulations using boundary prescribed motion rigid, with the floor constrained in five degrees of freedom (e.g., y-,z-translations and x-,y-,z-rotations).

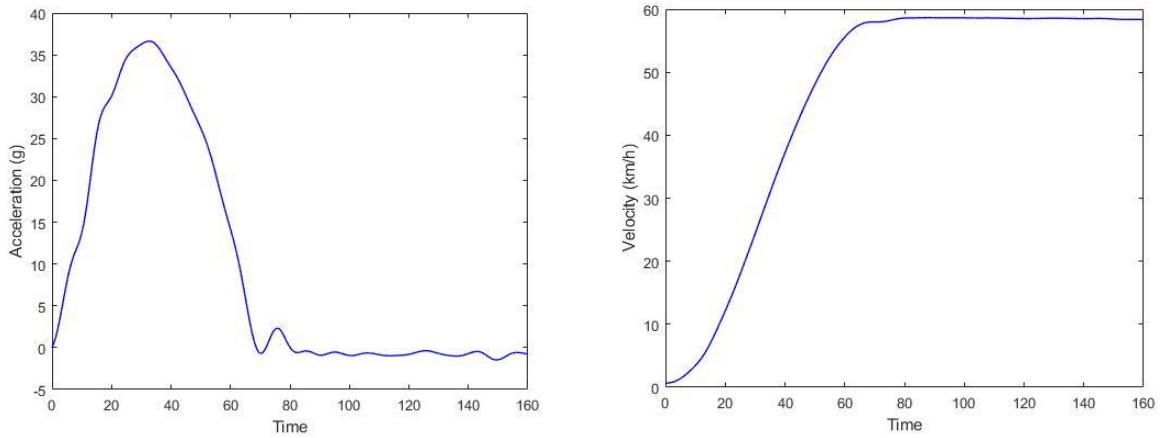

(a) x-Acceleration (b) x-Velocity

Figure 2: Sled pulse used in the experiment.

Simulation Workflow

The current study was sub-divided into three steps (Figure 3). The first step was validation of the seat using an unoccupied seat simulation. The second step was a simulation with a H3 Anthropomorphic Test Device (ATD) model for validation of an occupied seat. Model responses from the unoccupied seat and H3 simulations were compared to experimental data using normalized root mean squared deviation (NRMSD) (Kang et al., 2011). In the third step, the H3

was replaced with the GHBMC and simulated to evaluate its biofidelity using the NHTSA Biofidelity Ranking System (BRS) (Kang et al., 2020).

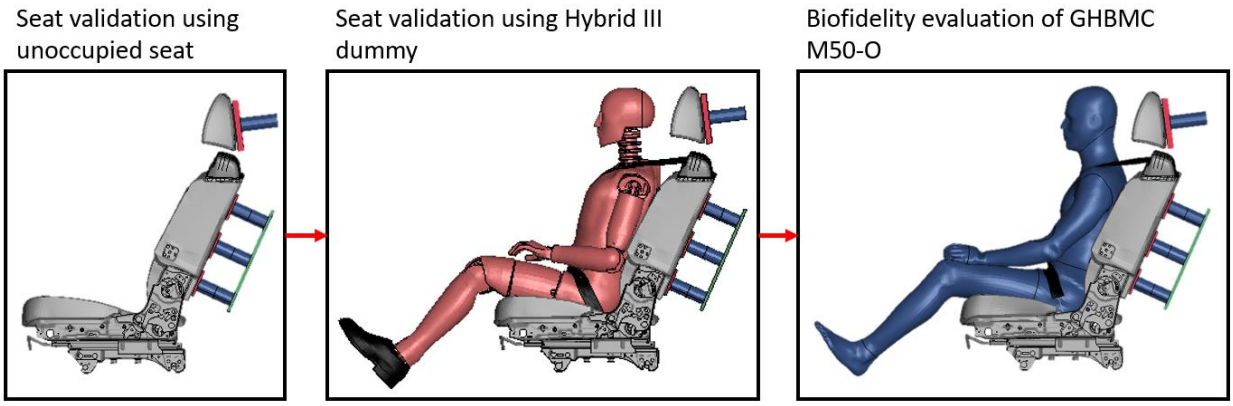

Figure 3: General workflow for the simulation study.

Unoccupied Seat Simulation

In order to validate connections in the seat frame and inertial seat loads, an unoccupied seat simulation was run and the seat reaction loads were measured in the x-axis direction from the load cells in the rigidized seatback structure (Figure 4).

(a) FE seat (b) Experimental seat.

Figure 4: Comparison of unoccupied seat setups between the simulation and experiment.

Hybrid III FE Model Simulation

Since the H3 FE model is geometrically similar to the experimental dummy, the boundary conditions from the experiment can be exactly replicated in the FE environment. The responses from the H3 can further help validate an occupied seat. Positioning parameters such as seated

height, thigh angle, leg angle, backset and topset were controlled using values gathered in experiments, to negate any differences in kinematics from model positioning (Figure 5).

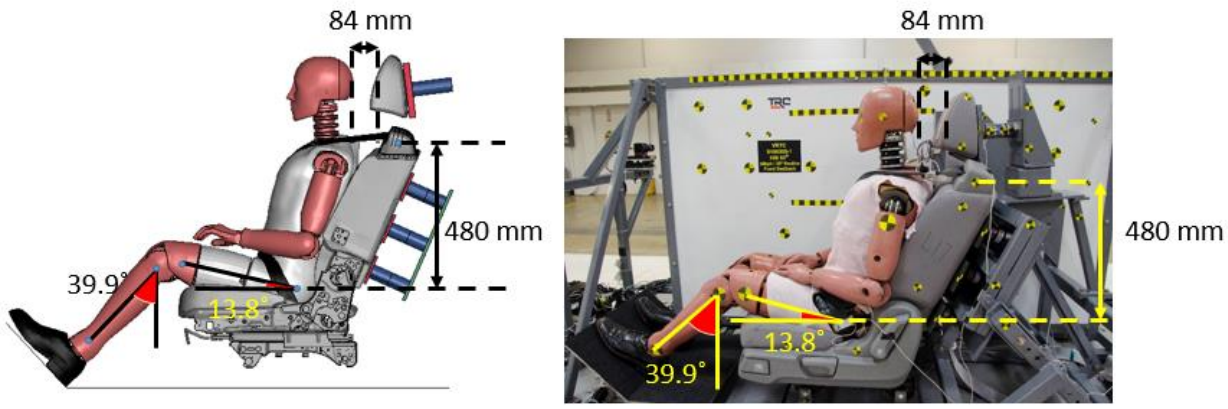

(a) H3 FE model (b) H3 ATD

Figure 5: Final position of H3 FE model compared to the H3 ATD used in experiments.

GHBMC M50-O Simulation

The average locations of anatomical bony landmarks obtained from the three PMHS tested in 25 degree seatback angle in a previous study (Kang et al., 2020, hereafter Kang study), were used to position the GHBMC. Pre-simulations were performed with gravity-based load body functions in both the x- and z-directions to settle the occupant onto the seat, while pre-compressing the seat cushion. The position was further optimized using the boundary prescribed final geometry function, to which the estimated final location of some nodes on the bony structures was provided. The final position (Figure 6a) was within one standard deviation of the PMHS mean for the parameters shown in Table 1. In order to match the average spinal curvature, mid-points on the anterior side of vertebral bodies for each PMHS were digitized from their reconstructed seated X-ray images (Figure 7). The spinal curvature of the GHBMC was then adjusted using boundary prescribed final geometry function to match the mean PMHS spinal curvature (Figure 8). Kinematic responses for head, T-spine, pelvis and lower extremities were obtained from interpolated nodes in their respective local coordinate systems, which were defined the same as in the Kang study. The inertial effects from the seat and the load cells from the unoccupied seat simulation were used to compensate the seat reaction loads from the GHBMC simulation.

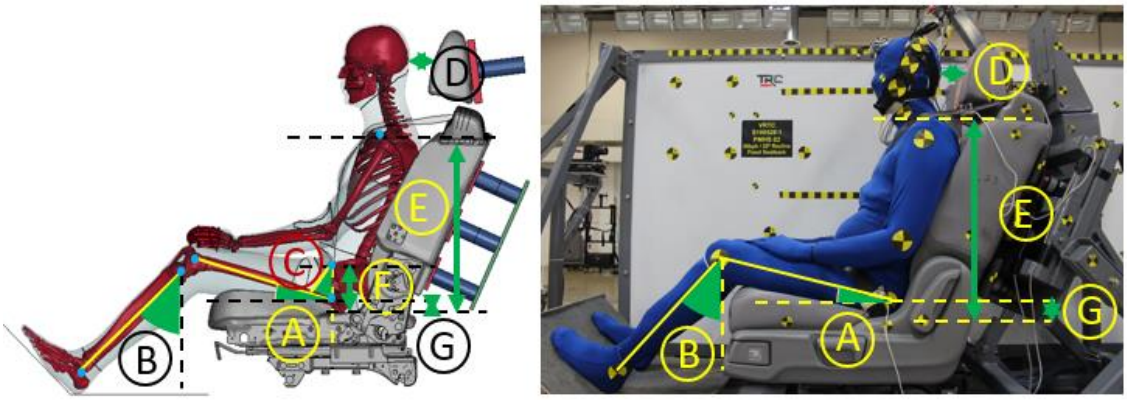

(a) GHBMC M50-O (b) PMHS

Figure 6: Final position of the GHBMC M50-O compared to PMHS used in experiments. The position parameters labeled A to G are shown in Table1.

Table 1: Positioning information for GHBMC

			PMHS Mean	PMHS Std. Dev.	GHBMC
A	Thigh Angle (deg)		12.6	0.9	13.0
B	Leg Angle (deg)		42.4	2.4	43.2
C	Pelvis Angle (deg)		32.1	2.4	31.8
D	Backset (mm)		79.3	4.5	79.3
E	Acromion (mm)	x	37.9	22.9	46.2
		z	519.7	21.2	507.6
F	ASIS (mm)	x	130.9	14.3	125.2
		z	117.6	13.8	125.5
G	GT (mm)	x	99.6	10.7	112.9
		z	20.7	5.5	23.5

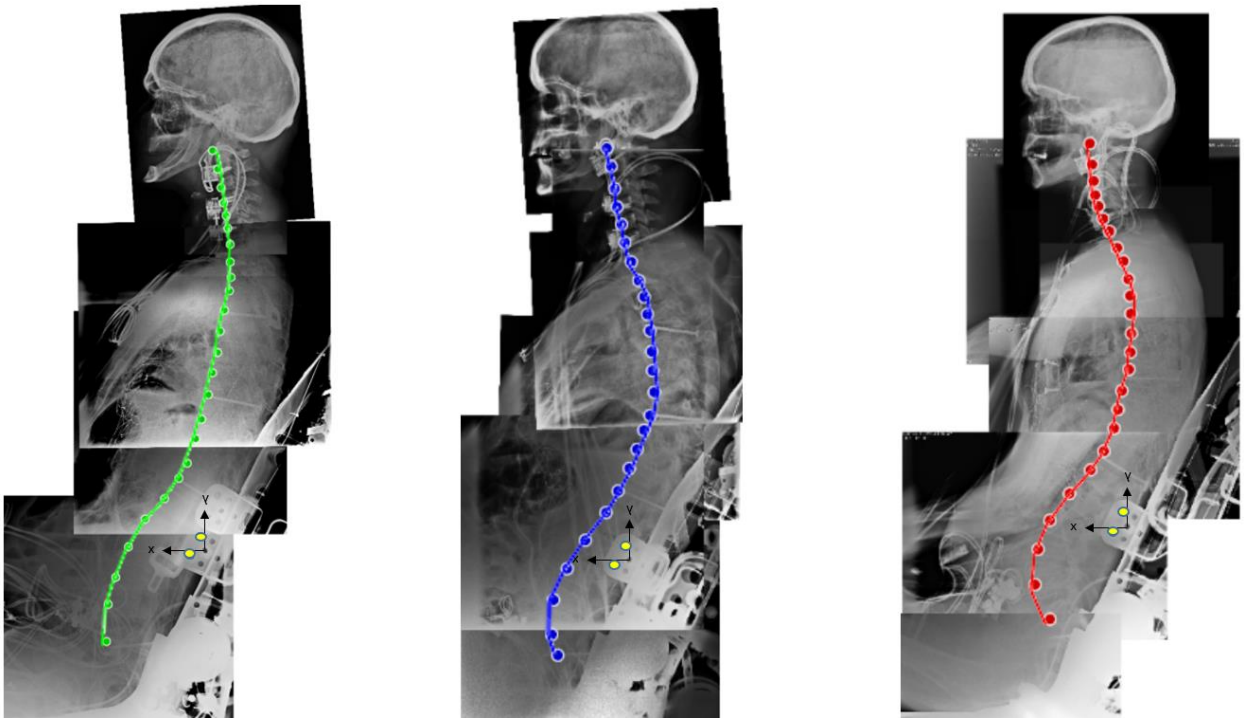

(a) HAV1902 (b) HAV1905 (c) HAV1908

Figure 7: Digitized mid points on anterior side of vertebral bodies in the three tested PMHS.

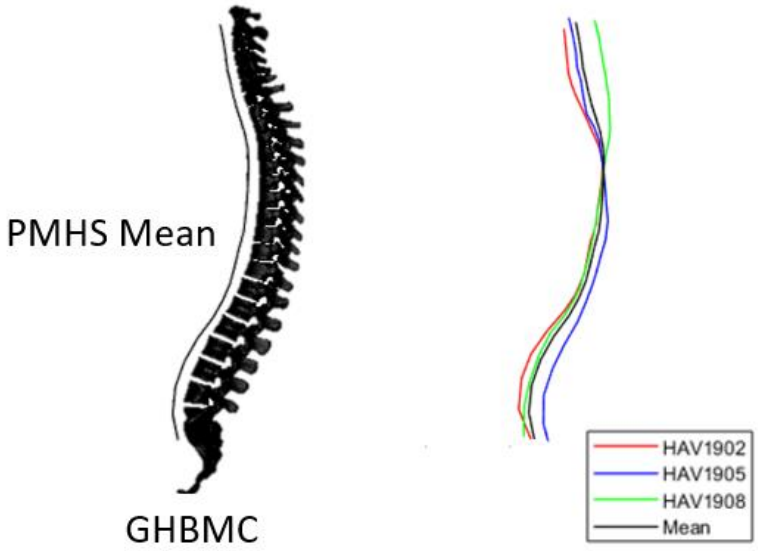

Figure 8: Mean spinal curvature of the GHBMC M50 occupant model.

RESULTS

NRMSD, BRS (B) and Dummy Phase Shift (DPS) scores have been indicated on the plots. BRS≤1, 1<BRS≤2 and BRS>2 indicate good, moderate and poor biofidelity, respectively.

Unoccupied Seat Simulation

Figures 9a-9c show the time-histories for seatback force in the x-direction as the sum of left and right load cells at the top, middle, and bottom respectively with NRMSD ranging from 8.3% to 14.0%. Figure 9d shows the time-history for total seatback force in the x-direction with a NRMSD of 9.7%.

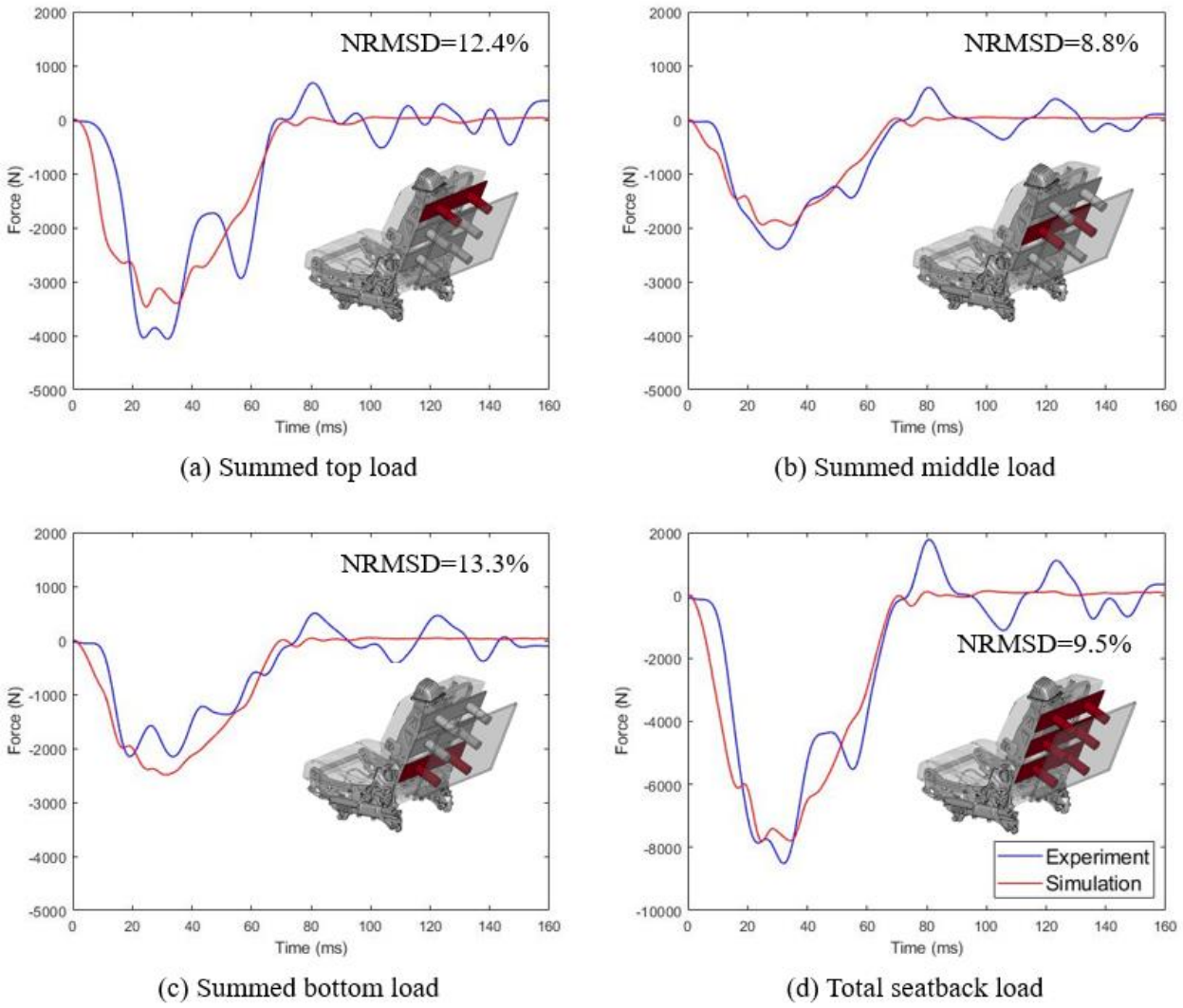

(a) Summed top load

(b) Summed middle load

(c) Summed bottom load

(d) Total seatback load

Figure 9: Seat reaction loads in the x-direction from the unoccupied seat simulation.

Hybrid III FE Model Simulation

Figures 10a and 10b show the time-histories of the x-acceleration of the chest and pelvis with NRMSD values of 9% and 12.6% respectively. Figure 10c shows the time-history for angular velocity of the pelvis about the y-axis with a NRMSD value of 8.1%.

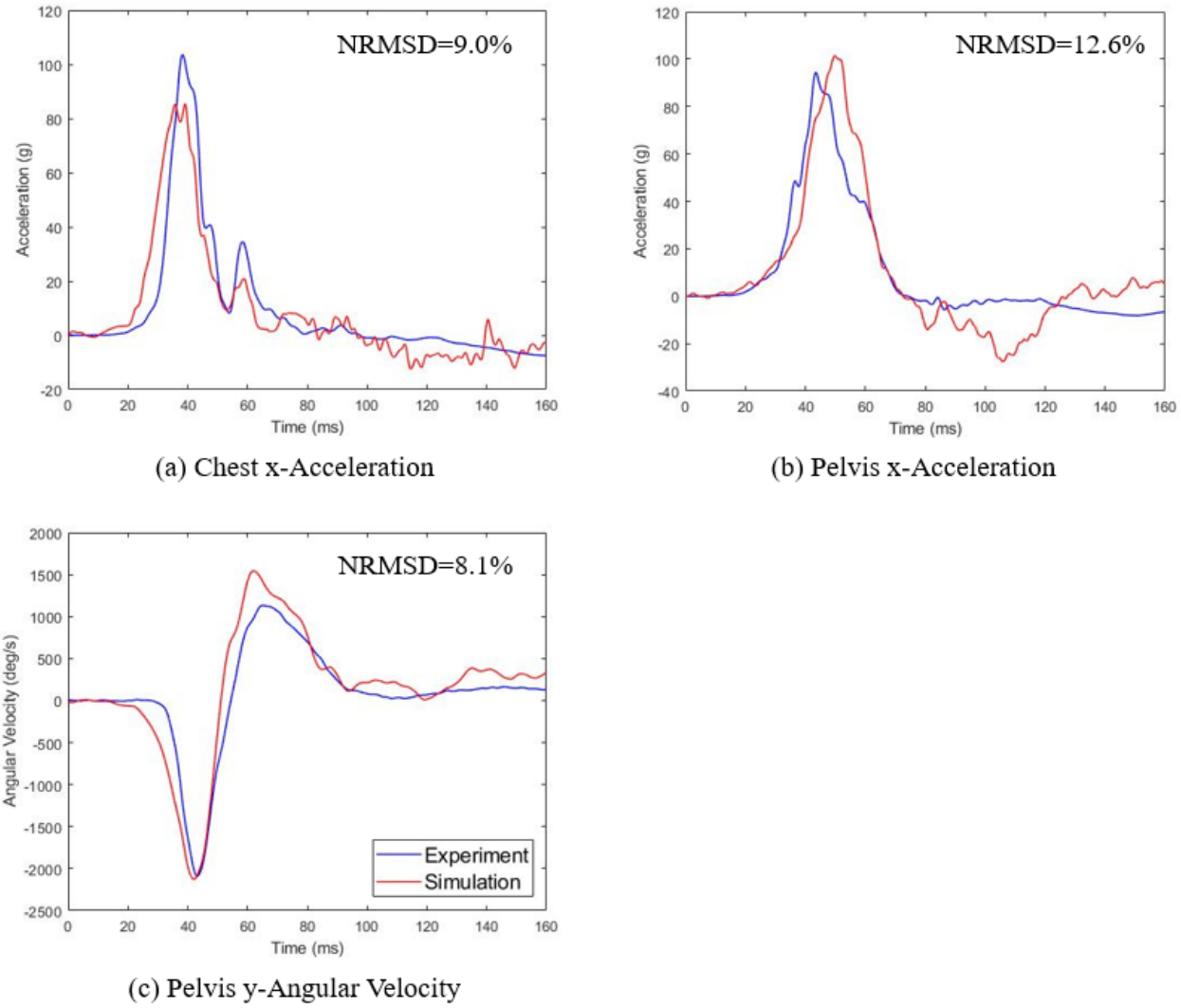

(a) Chest x-Acceleration

(b) Pelvis x-Acceleration

(c) Pelvis y-Angular Velocity

Figure 10: Chest and Pelvis Kinematics of Hybrid III.

The peak displacement of the target on the thigh in the direction of seatback foam compression matched well with the experiment, with a NRMSD of 12.2% for the time-history (Figure 11).

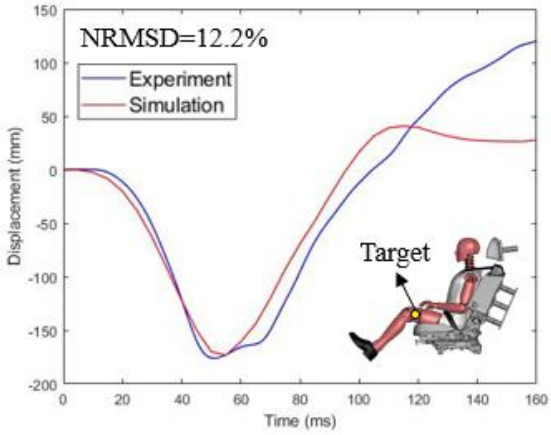

Figure 11: Target tracking on thigh of Hybrid III from high-speed video.

Figures 12a-12c show the time-histories for seatback force in the x-direction as the sum of left and right load cells at the top, middle, and bottom respectively with NRMSD ranging from 13.1% to 16.2%. Figure 12d shows the time-history for total seatback force in the x-direction with a NRMSD of 5.5%.

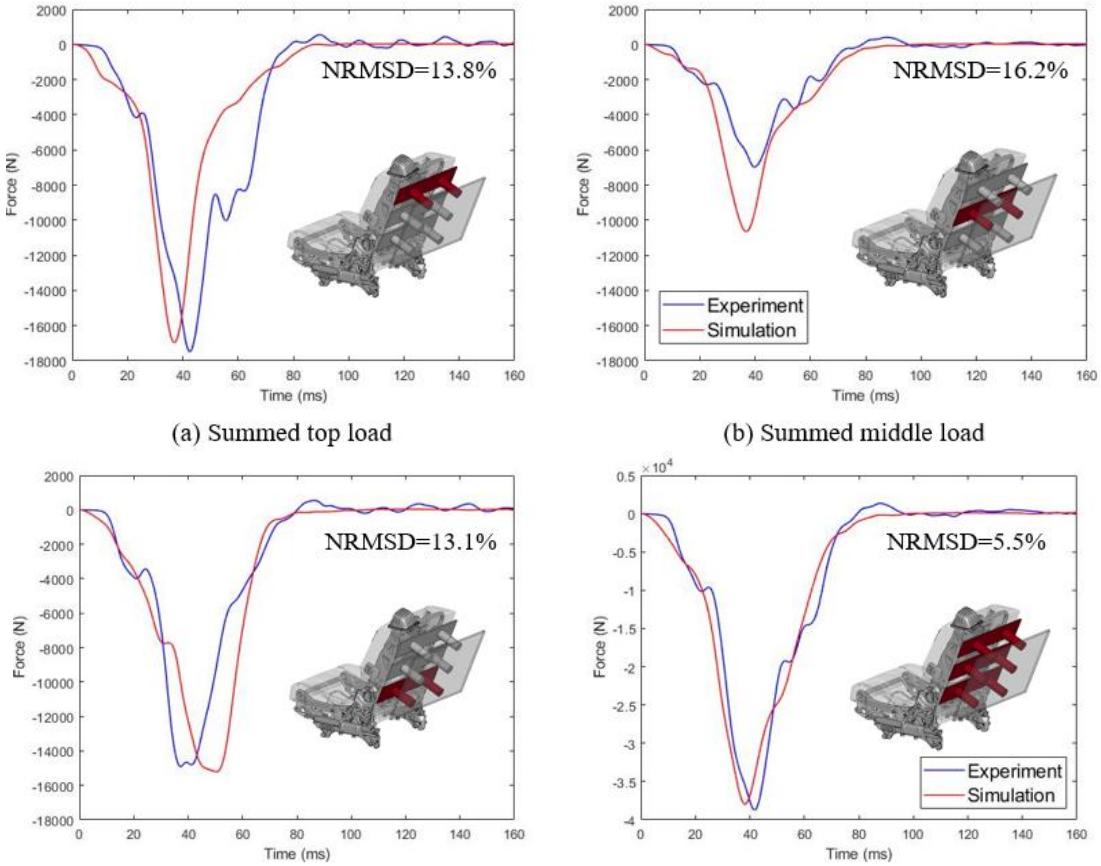

(a) Summed top load

(b) Summed middle load

(c) Summed bottom load

(d) Total seatback load

Figure 12: Seat reaction loads in the x-direction from the Hybrid III simulation.

GHBMC M50-O Simulation

Head Kinematics. Resultant head acceleration in the model had a moderate biofidelity with B=1.66 (Figure 13a). The head rotational characteristics of the model were similar to the PMHS mean (B=0.45) with head extending after contacting the head restraint (HR), followed by flexion in the rebound phase (Figure 13b). The peak global displacements of the head with respect to the sled in the x- (Figure 13c) and z-direction (Figure 13d) for the model were lower than the corresponding PMHS means by 61mm and 15mm respectively, resulting in poor biofidelity with B>2.

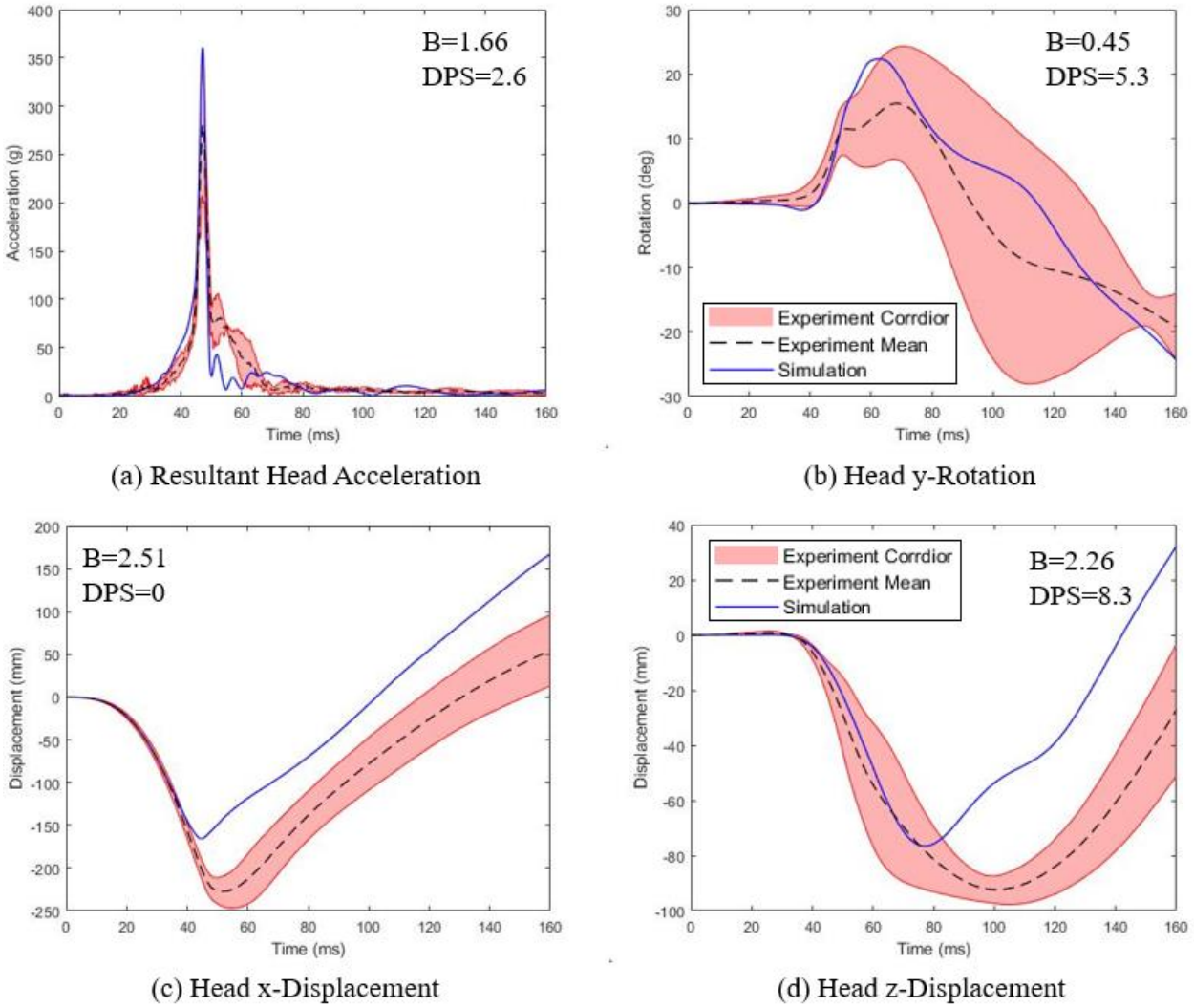

Figure 13: Head kinematics of the GHBMC M50-O. The PMHS had an average phase shift value of 1.97 and maximum phase shift value of 2.95.

T1 Kinematics. Resultant T1 acceleration of the model had a moderate biofidelity with B=1.44 (Figure 14a). Rotational characteristics for T1 in the model were similar to the experiment with BRS very close to 1 (Figure 14b). The peak global displacements of T1 with respect to the sled in the x- (Figure 14c) and z-direction (Figure 14d) for the model were lower than the corresponding PMHS means by 107.2mm and 25.8mm respectively, resulting in poor biofidelity with B>2.

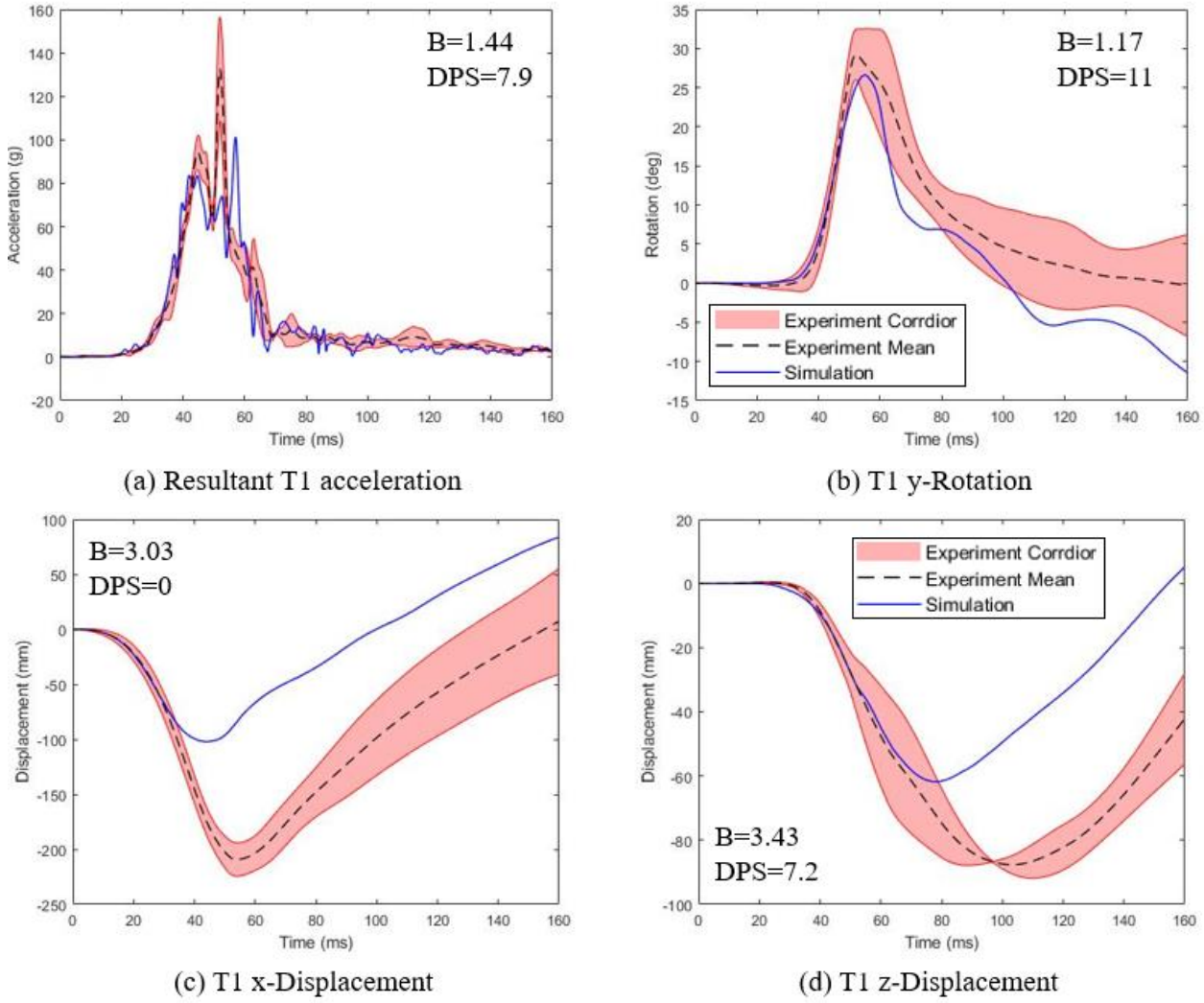

Figure 14: T1 kinematics of the GHBMC M50-O. The PMHS had an average phase shift value of 2.65 and maximum phase shift value of 3.95.

T4 Kinematics. The peak acceleration of T4 the x-direction in the model was about 39g lower than the PMHS mean, resulting in moderate biofidelity with B=1.79 (Figure 15a). However, the acceleration in the z-direction (Figure 15b) and angular velocity about the y-axis (Figure 15c) of T4 for the model had similar characteristics with B very close to 1.

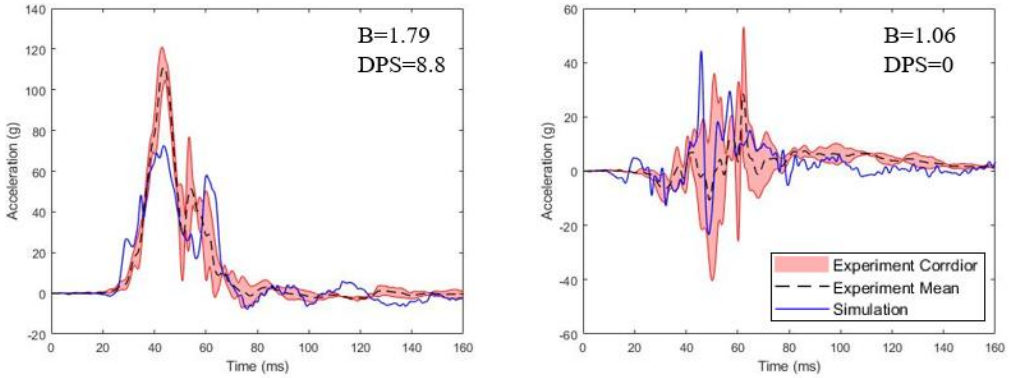

(a) T4 x-Acceleration

(b) T4 z-Acceleration

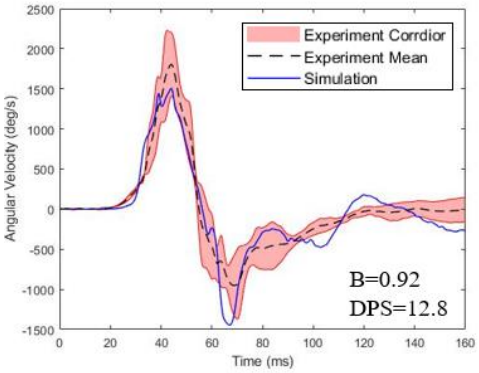

(c) T4 y-Angular Velocity

Figure 15: T4 kinematics of the GHBMC M50-O. The PMHS had an average phase shift value of 2.45 and maximum phase shift value of 3.70.

T8 Kinematics. The acceleration of T8 in the x- (Figure 16a) and z-direction (Figure 16b) in the model had moderate biofidelity with $1<B\leq2$.

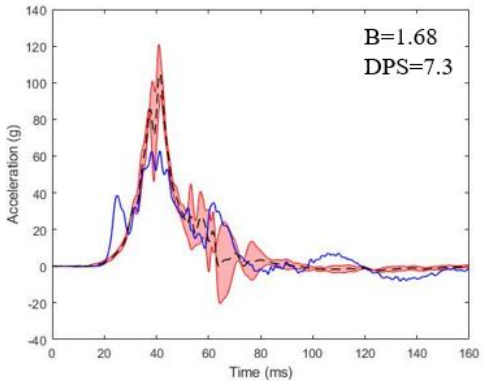

(a) T8 x-Acceleration

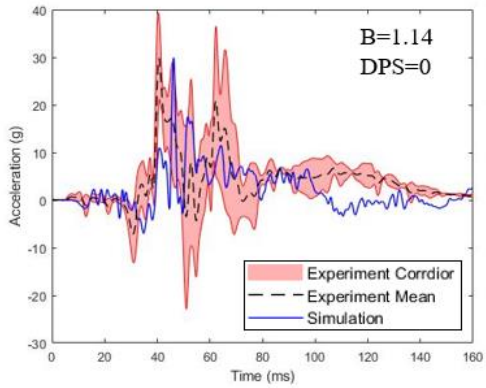

(b) T8 z-Acceleration

Figure 16: T8 kinematics of the GHBMC M50-O. The PMHS had an average phase shift value of 2.25 and maximum phase shift value of 3.40.

T12 Kinematics. The acceleration of T12 in the x- (Figure 17a) and z-direction (Figure 17b), and its angular velocity about the y-axis (Figure 17c) in the model had moderate biofidelity with 1<B≤2.

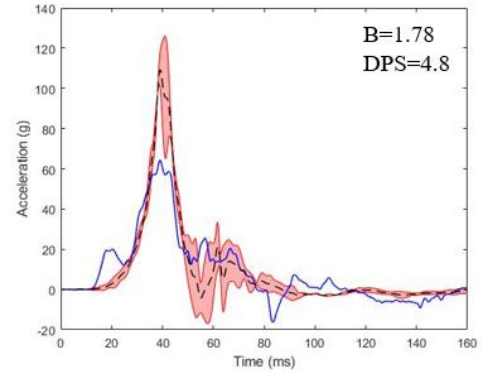

(a) T12 x-Acceleration

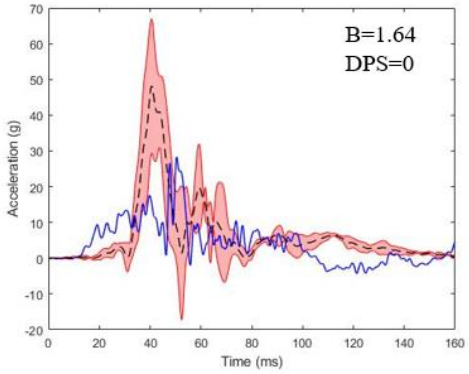

(b) T12 z-Acceleration

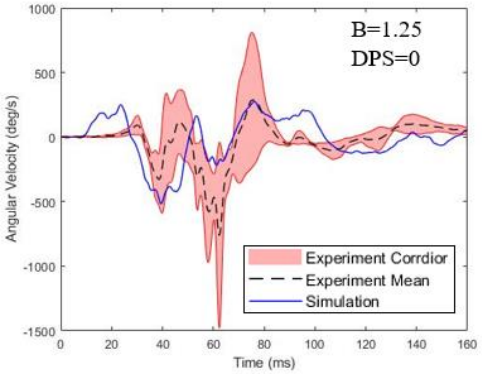

(c) T12 y-Angular Velocity

Figure 17: T12 kinematics of the GHBMC M50-O. The PMHS had an average phase shift value of 3.12 and maximum phase shift value of 4.65.

Normalized Chest Deflection. Figure 18 shows the anterior-to-posterior chest deflection of the GHBMC, normalized by half chest depth. Moderate biofidelity (B=1.93) was observed in the GHBMC, as there was no expansion phase unlike the PMHS.

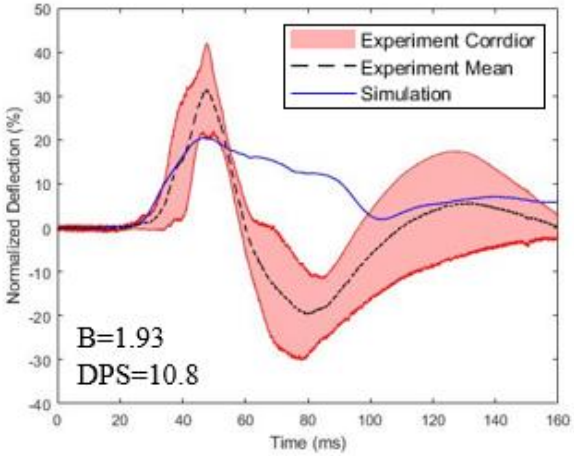

Figure 18: Normalized anterior-to-posterior chest deflection of the GHBMC M50-O. The PMHS had an average phase shift value of 5.23 and maximum phase shift value of 7.85.

Pelvis Kinematics. The peak resultant pelvis acceleration in the model was about 55g lower than the experimental mean, resulting in moderate biofidelity with B=1.86 (Figure 19a). The model's peak pelvis flexion was more than twice as high as the PMHS mean, resulting in poor biofidelity with B>2 (Figure 19b). The peak global displacements of pelvis with respect to the sled in the x- (Figure 19c) and z-direction (Figure 19d) for the model were lower than the corresponding PMHS means by 71.6mm and 42.6mm respectively, resulting in poor biofidelity with B>2.

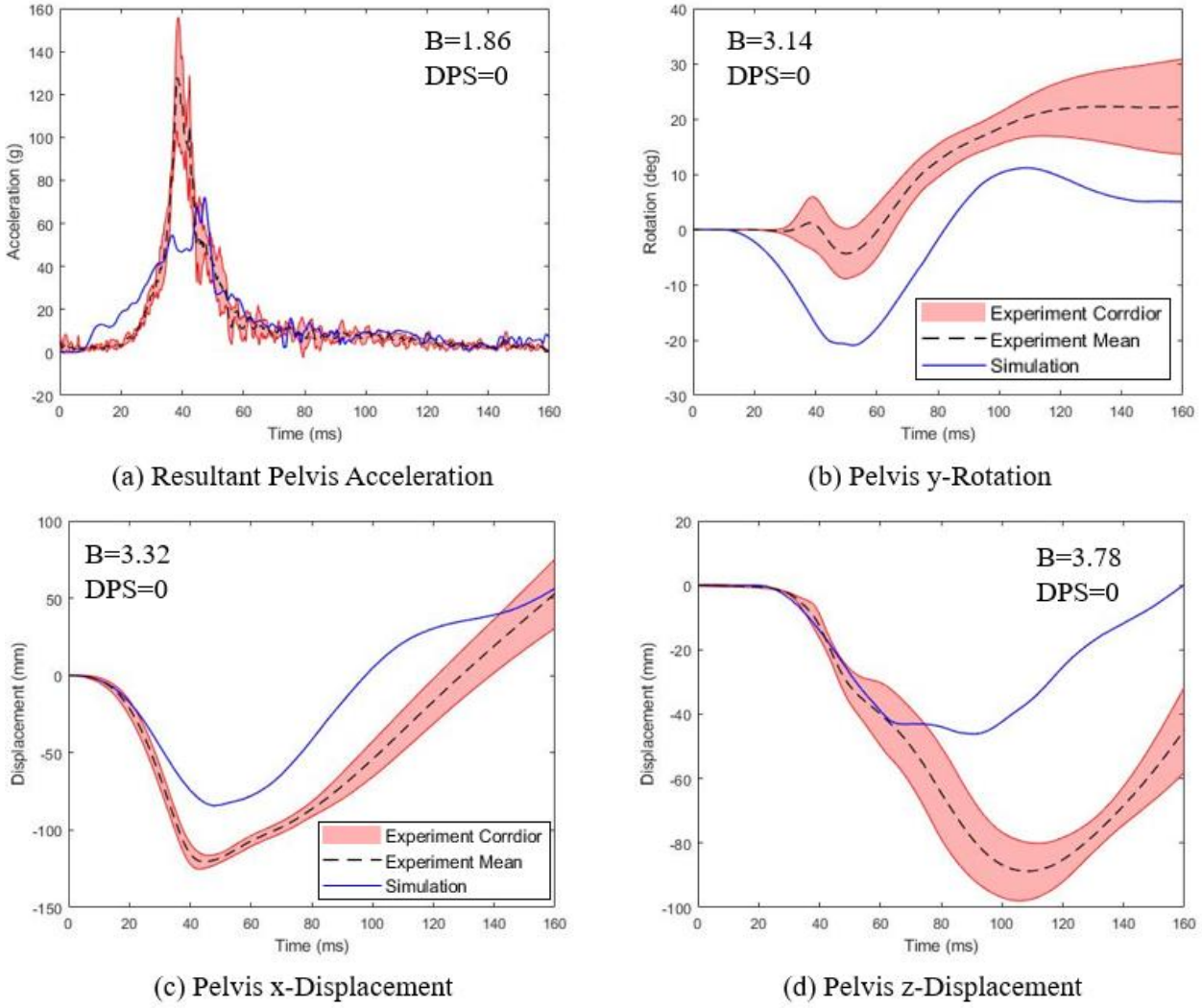

Figure 19: Pelvis kinematics of the GHBMC M50-O. The PMHS had an average phase shift value of 2.23 and maximum phase shift value of 3.35.

Lower extremities. The B values for resultant accelerations of the left and right femurs (Figures 20a and 20b) of the model were 1.74 and 2.25, indicating moderate and poor biofidelity respectively. The resultant accelerations of the tibiae (Figures 20c and 20d) of the model had B values close to 1. The angular velocities about the y-axis for all lower extremities (Figures 21e-21h) of the model ranged from moderate to poor biofidelity ($1.92 \leq B \leq 2.82$).

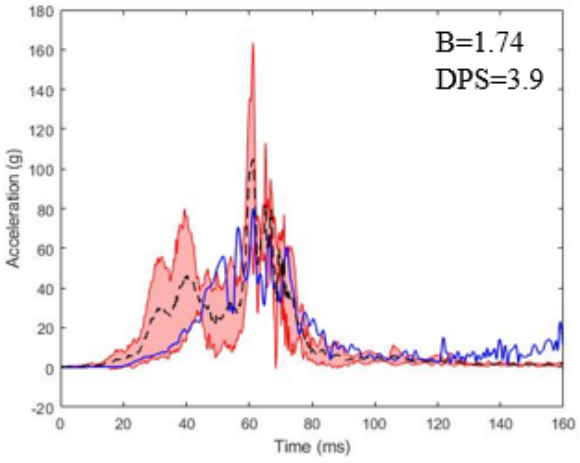

(a) Resultant Left Femur Acceleration. The PMHS had an average phase shift value of 1.82 and maximum phase shift value of 2.75.

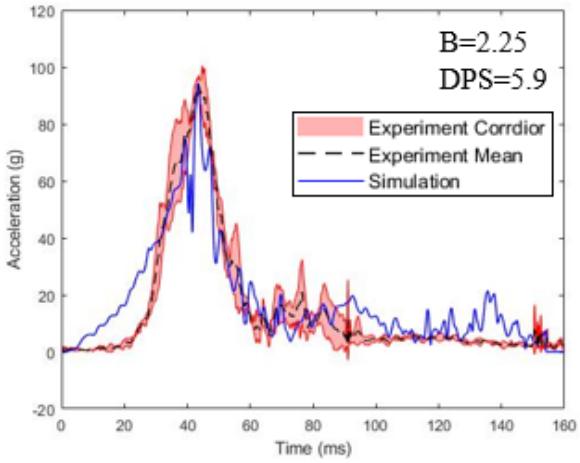

(b) Resultant Right Femur Acceleration. The PMHS had an average phase shift value of 1.52 and maximum phase shift value of 2.25.

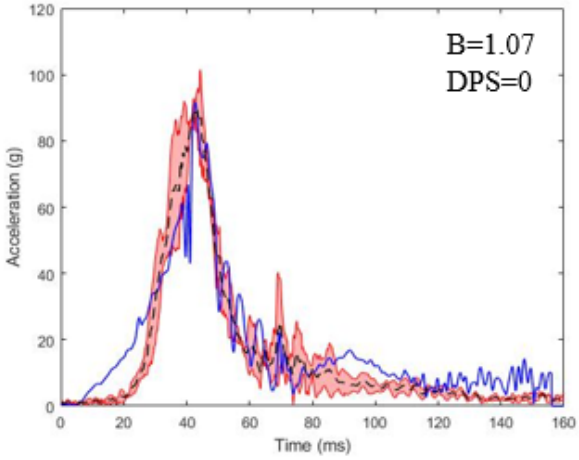

(c) Resultant Left Tibia Acceleration. The PMHS had an average phase shift value of 7.55 and maximum phase shift value of 11.30.

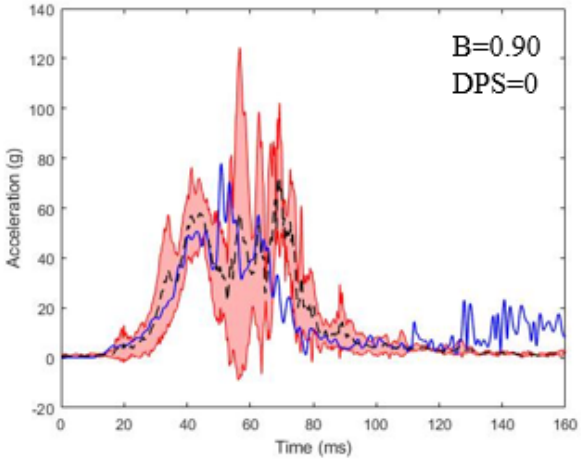

(d) Resultant Right Tibia Acceleration. The PMHS had an average phase shift value of 3.95 and maximum phase shift value of 5.95.

Figure 20: Lower extremity linear kinematics of GHBMC M50-O.

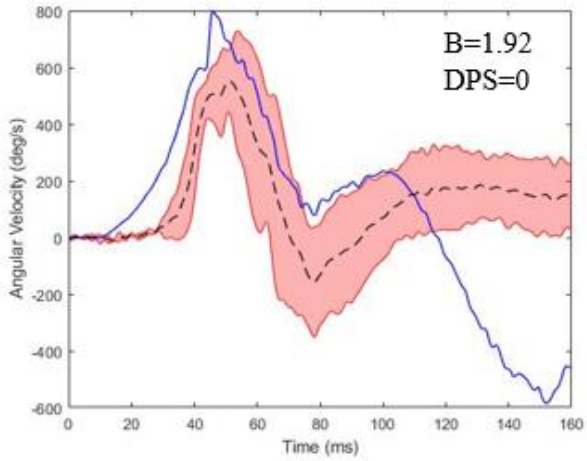

(e) Left femur y-Angular Velocity. The PMHS had an average phase shift value of 1.82 and maximum phase shift value of 2.75.

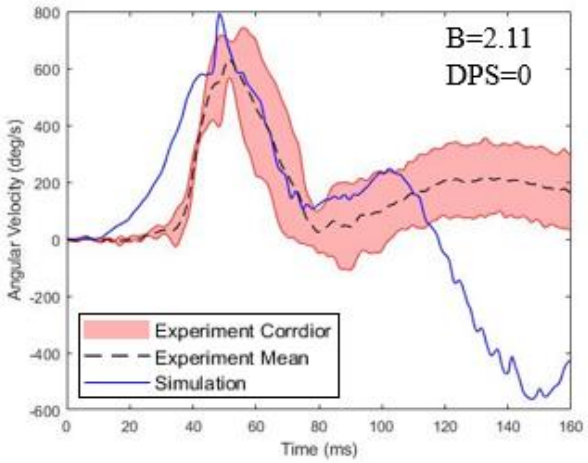

(f) Right Femur y-Angular Velocity. The PMHS had an average phase shift value of 1.52 and maximum phase shift value of 2.25.

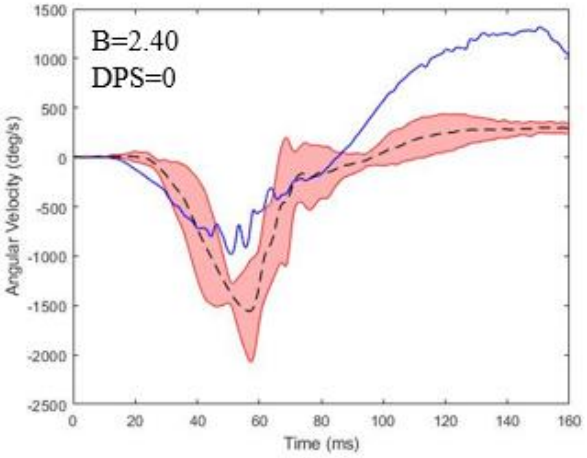

(g) Left Tibia y-Angular Velocity. The PMHS had an average phase shift value of 7.55 and maximum phase shift value of 11.30.

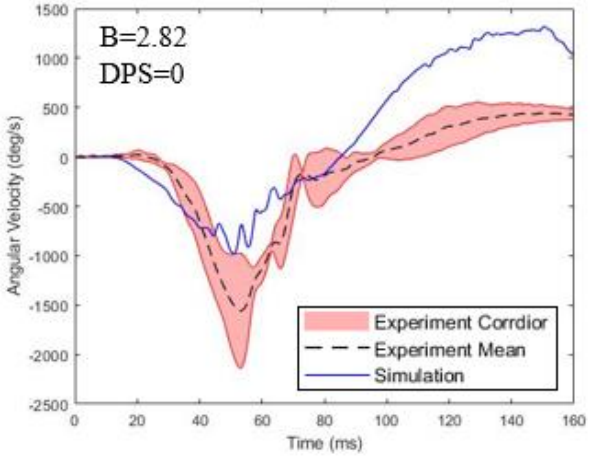

(h) Right Tibia y-Angular Velocity. The PMHS had an average phase shift value of 3.95 and maximum phase shift value of 5.95.

Figure 21: Lower extremity angular kinematics of GHBMC M50-O.

Seat reaction loads. HR force in the x-direction (Figure 22) in the model was 1.8kN higher than the PMHS mean, with poor biofidelity (B=3). Seatback forces in the x-direction as the sum of left and right load cells at the top (Figure 23a), middle (Figure 23b), and bottom (Figure 23c) exhibited poor biofidelity (2.44≤B≤5.25). Total seatback force in the x-direction (Figure 23d) for the model was 14.5kN lower than the PMHS mean with a poor biofidelity (B=4.32).

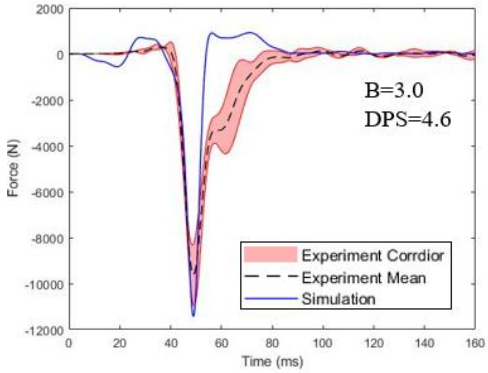

Figure 22: HR load in the x-direction from the GHBMC M50-O simulation. The PMHS had an average phase shift value of 1.90 and maximum phase shift value of 2.85.

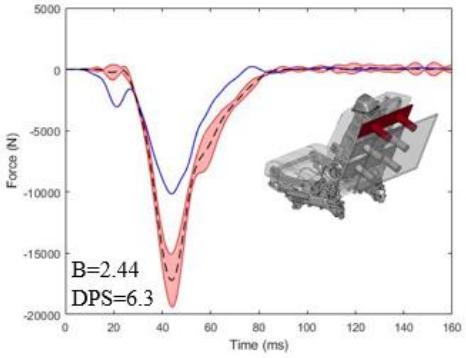

(a) Summed top load. The PMHS had an average phase shift value of 1.88 and maximum phase shift value of 2.80.

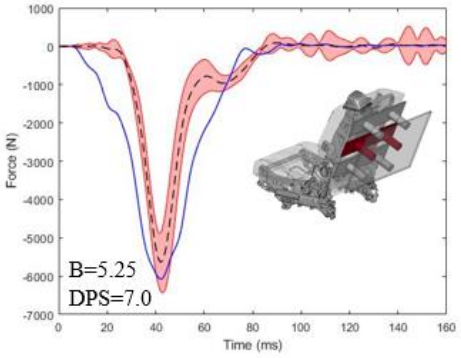

(b) Summed middle load. The PMHS had an average phase shift value of 2.27 and maximum phase shift value of 3.40.

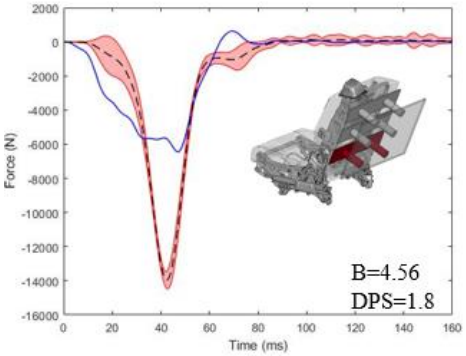

(c) Summed bottom load. The PMHS had an average phase shift value of 1.78 and maximum phase shift value of 2.65.

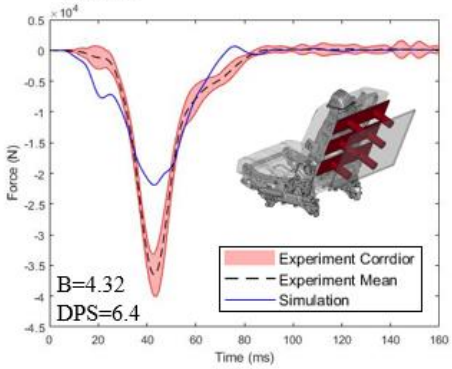

(d) Total seatback load. The PMHS had an average phase shift value of 1.70 and maximum phase shift value of 2.55.

Figure 23: Seatback loads in the x-direction from the GHBMC M50-O simulation.

DISCUSSION

The main objective of this study was to evaluate the biofidelity of the GHBMC M50-O occupant model in a high-speed rear-facing scenario. In order to ensure reproducibility of the FE seat, an additional effort was made to validate the seat using a high-speed rear facing unoccupied seat simulation and a Hybrid III simulation.

Seat Validation using Unoccupied Seat Simulation

The responses in the model seemed to follow the trend of the sled pulse as the connection between the seatback structure and the sled floor was perfectly rigid, unlike the experiment, where some delay was observed in the acceleration of the load plates and the floor, due to small relative motions at the joint shown in Figure 24. High-speed video of the experiment also revealed that there was some amount of plate rotation about the y-axis, which could affect the reaction loads measured by the load cells. The FE model of the seatback structure needs to be improved to mimic the small rotational behavior of the plates.

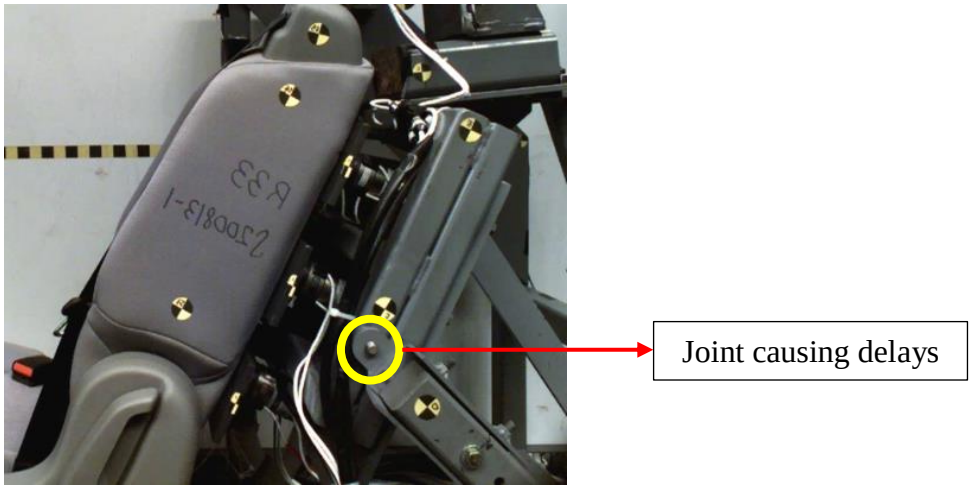

Figure 24: Physical connection in the seatback structure in the experiment.

Apart from the seatback structure, the differences in the seatback loads between the FE seat and the physical seat could be due to few reasons: 1) difference in stiffness of seatback parts contacting the top and middle plates, 2) stiffer moment-rotation at the seat recliner that would prevent the seat from rotating enough to generate the loads seen in the experiment, and 3) different contact friction between the parts of the seat frame and the plates. While these aspects of the seat model could be further refined, the NRMSD for total seatback load for the model was less than 10% with the current setup, indicated the current seat model is effective for use in evaluating human body models in a high-speed rear-facing scenario.

Seat Validation using H3 Dummy

The kinematics of the model (Figures 10a-10c) had NRMSD<13% with respect to the experimental responses. Target tracking on the thigh revealed equivalent foam compression as in

the experiment (Figure 11), thereby confirming the acceptable use of the current foam loading properties in the model. Although the total seatback load (Figure 12d) was matched (NRMSD=5.5%), summed loads at the top (Figure 12a), middle (Figure 12b) and bottom (Figure 12c) for the simulation did not match the experimental loads. This difference in load distribution could be attributed to the lack of reproducibility in the FE H3 model from its interaction with the seatback. Since H3 is a frontal ATD, it might not have been validated in this fixed seat, rear impact condition. With this limitation, NRMSD for load distribution ranged from 13.1% to 16.2%.

Biofidelity Evaluation of GHBMC

Head Interaction with HR. Head kinematics are sensitive to position (adjustment) of the HR (Hassan et al., 2018) and small HR movements during their interaction. Since the HR was rigidly constrained to the sled floor in the simulation, the small rotations about the y-axis (approximately 5 degree) were not observed unlike the experiment. This ensured better coupling between the head and HR during the impact, thereby generating a higher resultant acceleration than the PMHS mean (Figure 13a). This was also indicated by the higher HR load in the x-axis direction (Figure 22).

Head and T1 kinematics. Head (Figure 13b) and T1 (Figure 14b) rotations for the GHBMC fell within the biomechanical corridors. This outcome was consistent with the fact that the head to T1 region has been previously validated, although at low-severity rear impacts (Fice et al., 2011). Poor biofidelity of the x-axis displacement (Figure 13c) of the head could be due to a less-compliant skull or reduced ramping that prevented the head from traveling rearward along the HR, whereas for T1 (Figure 14c) the poor biofidelity score could be due to a stiffer neck region. A difference in neck flexibility could affect the head to T1 kinematics (Katagiri et al., 2019). Relative head to T1 rotations between the GHBMC and PMHS will be compared to give us a better idea about the neck flexibility.

Ramping Behavior. Ramping is an important parameter representative of occupant-seat coupling (Kang et al., 2020). The ramping up motion of the GHBMC that was indicated by the z-axis displacements of the head (Figure 13d), T1 (Figure 14d) and pelvis (Figure 19d) was lower than the PMHS, with poor biofidelity (B scores>2). Pelvis ramping was mainly restricted by the lap belt, as seen through the higher peak lap belt force compared to the experiments (Figure A2). Head and T1 ramping for the GHBMC were partly affected by the lower ramping of pelvis, due to the continuity between head and pelvis through the spine. When the GHBMC simulation was run without a seatbelt, the pelvis ramped up much more (Figure A3), suggesting that there might be an issue with the belt properties used in the model, which could not be captured from the H3 simulation due to lack of biofidelity of the H3. Unlike the PMHS experiments, abdominal contents of the GHBMC did not translate upwards and expansion of the chest in the rebound phase was not observed (Figure 18). The material properties, connections and contacts of the abdominal organs and flesh need to be explored further.

Spine Straightening Behavior. Rotations and angular velocities about the y-axis are representative of spine straightening behavior (Kang et al., 2020). Like in the experiments, as the GHBMC translated rearward into the seatback, T1 (Figure 14b) and T4 (Figure 15c) rotated rearward, while T12 (Figure 17c) and pelvis (Figure 19b) rotated forward. Thus, the straightening characteristics of the thoracic and lumbar spine of the GHBMC were similar to those observed in the PMHS. The

seat reaction loads could be possibly affected by the flexibility of the spine and pelvis (Katagiri et al., 2019), as some energy of the impact is dissipated in rotation. For the H3 simulation, pelvis y-angular velocity matched the experimental response (Figure 10c), which subsequently resulted in reasonably summed bottom load (Figure 12c). However, for the GHBMC, the pelvis rotation was much higher than the PMHS mean so that bottom summed load became smaller than PMHS (Figure 23c). The increased pelvis rotation could be due to higher inertia of the GHBMC lower extremities and flexibility of the lumbar spine.

Occupant Coupling with Seatback. Accelerations and displacements in the x-axis direction also govern the amount of coupling between the occupant and the seatback (Kang et al., 2020). The displacements of T1 (Figure 14c) and pelvis (Figure 19c) with respect to the sled in the x-axis direction for the GHBMC were lower than the PMHS mean, with poor biofidelity. The x-axis accelerations of T4 (Figure 15a), T8 (Figure 16a) and T12 (Figure 17a) of the GHBMC were also lower than the PMHS, with moderate biofidelity. The lower coupling with the seatback could be due to lower stiffness of bones and flesh in the thoracic and pelvis region. Moreover, lower normalized deflection of the chest in the anterior-to-posterior direction (Figure 18) confirmed that the thoracic region was not biofidelic for rear impacts and the rib deformations might have to be modeled better. The lower seatback coupling for the thoracolumbar spine and the pelvis was also indicated by the low summed top (Figure 23a) and bottom (Figure 23c) loads. Low seatback loads for the GHBMC models have been previously observed in moderate-speed rear impacts, as compared to the PMHS (Katagiri et al., 2019).

Lower Extremities Kinematics. Resultant accelerations of the femurs and tibiae (Figures 20a-20d) had BRS scores ranging from good to moderate. However, rotational characteristics of the lower extremities (Figures 21e-21f) deviated from biofidelity in the rebound phase, with a significant kicking-up motion (Figure A1) seen in the tibiae, which has been previously observed in moderate-speed rear impacts (Katagiri et al., 2019). This could be due to a lower y-axis rotational stiffness at the knee joints in the GHBMC as compared to the PMHS.

LIMITATIONS AND FUTURE WORK

The occupant responses could be affected by the seat and sled characteristics. Seat recline characteristics should be fine-tuned, as small seatback rotation during the impact may affect the seatback loads. The connections in the seatback structure were completely rigid in the FE model used in this study, thereby not allowing any rotational motion. Small rotations in the load plates could affect their contact with the seat frame. Physical joint connections with rotational stiffness could be introduced in the seatback structure. A target point on the thigh was tracked in the H3 simulation for verifying the accuracy of foam properties. It would have been more logical to track a target point on the pelvis since it interacts directly with the seatback foam, but this target was hidden behind the lap belt in the high-speed video. The inertial seat loads from the unoccupied seat and H3 simulations were reasonably matched, but the differences in peak loads and time-delay in responses could be further improved if the seat frame and foam properties were further validated using compression tests at strain rates typically observed in the impact. Overall position and

posture of the GHBMC were close to the PMHS mean, but advanced morphing techniques may need to be attempted in the future, in order to better match key anatomical landmarks.

CONCLUSIONS

This study presented the biofidelity evaluation of the GHBMC M50-O in a 56km/h rear-facing seat in frontal-impact scenario in addition to validation of an OEM seat and the boundary conditions. Preliminary conclusions from this study are as follows:

- The total seatback loads from the unoccupied seat and H3 simulations were within 10% of the experimental loads.
- The GHBMC exhibited good (BRS≤1) to moderate biofidelity (1<BRS≤2) for the rotational kinematics about the y-axis for head and T1 during head interaction with HR, however, poor biofidelity (BRS>2) were recorded for their displacements in the x-axis direction.
- Spine straightening was observed in the GHBMC similar to PMHS mean with T1, T4 and T8 undergoing extension and T12 and pelvis undergoing flexion, while the GHBMC translated rearward into the seatback cushion.
- Pelvis and lower extremities exhibited poor biofidelity (BRS>2) for their rotational kinematics.

ACKNOWLEDGEMENTS

We would like to acknowledge TS-Tech Americas, Inc for providing the FE model of the OEM seat. We would also like to thank the Ohio Supercomputer Center for providing resource units for running our simulations. Finally, we would like to appreciate all the faculty, staff and students at the Injury Biomechanics Research Center for assisting with various aspects of the project and providing valuable insights on the same.

REFERENCES

Fice, Jason B., Duane S. Cronin, and Matthew B. Panzer. "Cervical spine model to predict capsular ligament response in rear impact." *Annals of biomedical engineering* 39.8 (2011): 2152-2162.

Hassan, Mohamed TZ, and S. A. Meguid. "Effect of seat belt and head restraint on occupant's response during rear-end collision." *International Journal of Mechanics and Materials in Design* 14.2 (2018): 231-242.

Jorlöv, Sofia, Katarina Bohman, and Annika Larsson. "Seating positions and activities in highly automated cars–a qualitative study of future automated driving scenarios." *International Research Conference on the Biomechanics of Impact*. 2017.

Kang, Yun-Seok, et al. "Biomechanical responses and injury assessment of post mortem human subjects in various rear-facing seating configurations." *Stapp car crash journal* 64 (2020): 155-212.

Katagiri, Maika, et al. "Biofidelity Evaluation of GHBMC Male Occupant Models in Rear Impacts." *Proceedings of the ICROBI Conference, Florence, Italy*. 2019.

Kitagawa, Yuichi, et al. *Occupant kinematics in simulated autonomous driving vehicle collisions: influence of seating position, direction and angle*. No. 2017-22-0005. SAE Technical Paper, 2017.

White, Nicholas A., et al. "Cross-sectional neck response of a total human body FE model during simulated frontal and side automobile impacts." *Computer methods in biomechanics and biomedical engineering* 18.3 (2015): 293-315.

Y.-S. Kang, K. Moorhouse, and J. H. Bolte, "Measurement of Six Degrees of Freedom Head Kinematics in Impact Conditions Employing Six Accelerometers and Three Angular Rate Sensors (6aω Configuration)," J. Biomech. Eng., vol. 133, no. 11, p. 111007, 2011.

APPENDIX

Figure A1: General kinematics of the GHBMC compared to one of the PMHS tested.

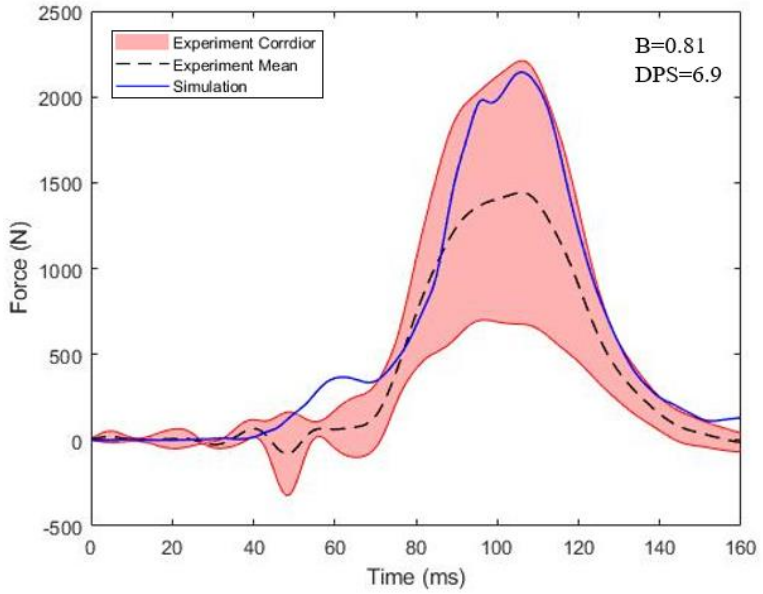

Figure A2: Lap belt load in GHBMC. The PMHS had an average phase shift value of 4.15 and maximum phase shift value of 6.20.

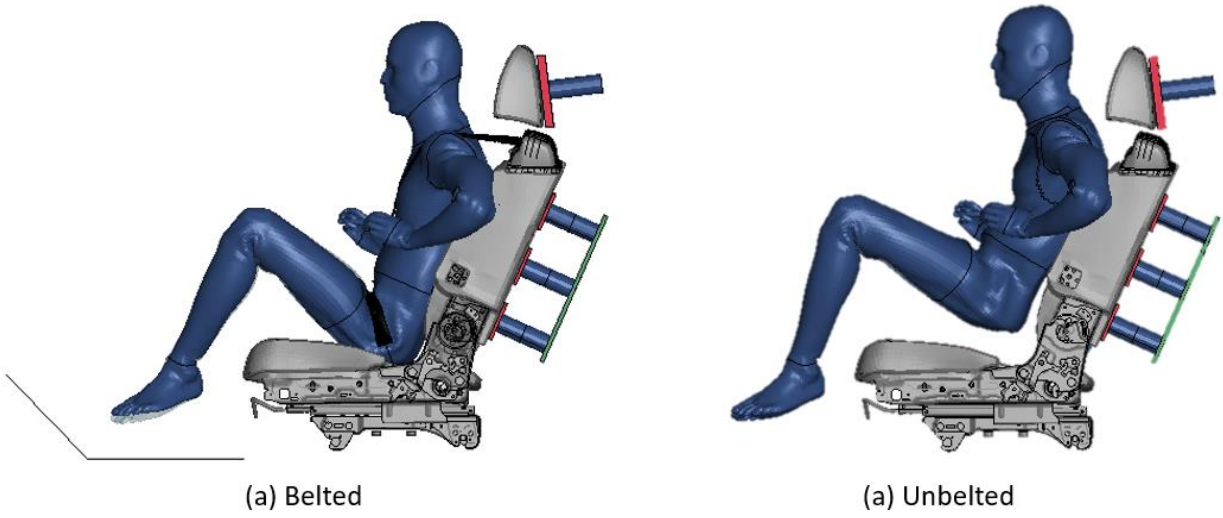

Figure A3: Comparison of ramping between belted and unbelted GHBMC at 110 ms.